

Mapping the three-body system – decay time and reversibility

H. J. Lehto^{1*}, S. Kotiranta¹, M. J. Valtonen¹, P. Heinämäki¹, S. Mikkola¹, A. D. Chernin^{1,2}

¹*Department of physics and Tuorla observatory, University of Turku, Finland*

²*Sternberg Astronomical Institute, Moscow university, 119899, Moscow Russia*

Accepted Received . . . ; in original form 2008 February 28

ABSTRACT

In this paper we carry out a quantitative analysis of the three-body systems and map them as a function of decaying time and initial configuration, look at this problem as an example of a simple deterministic system, and ask to what extent the orbits are really predictable. We have investigated the behavior of about 200 000 general Newtonian three body systems using the simplest initial conditions. Within our resolution these cover all the possible states where the objects are initially at rest and have no angular momentum. We have determined the decay time-scales of the triple systems and show that the distribution of this parameter is fractal in appearance. Some areas that appear stable on large scales exhibit very narrow strips of instability and the overall pattern, dominated by resonances, reminds us of a traditional Maasai warrior shield. Also an attempt is made to recover the original starting configuration of the three bodies by backward integration. We find there are instances where the evolution to the future and to the past lead to different orbits, in spite of time symmetric initial conditions. This implies that even in simple deterministic systems there exists an Arrow of Time.

Key words: celestial mechanics – methods: N -body simulations

1 INTRODUCTION

Dynamical interaction of multiple objects is common in physics and astronomy. It occurs over a huge range of scales from atoms in molecules to galaxies. If we know the interaction potential, then it is possible in principle to calculate the evolution of such a system. As is well known, systems of this kind tend to be chaotic, and so is the solution of the three-body problem (Prigogine & Stengers 1984; Aarseth et al. 1994).

The two body problem in a Newtonian gravitational potential is simple enough to be solvable in a closed form. Adding a third body to the system complicates matters by producing, in general, non-analytic solutions. Over a century ago (Poincaré 1892) realized the chaotic nature of the few body system, but only with the advance of computer power and more sophisticated algorithms has it been possible to give more quantitative statements in the three body problem (Heggie 1975; Mikkola 1994; Aarseth et al. 1994).

Here we introduce a simple way to illustrate and study the fractal nature of the general three body system. The method we describe provides an important tool for visual and qualitative studies of the three body problem. It allows us to handle and analyze *all* possible three body configura-

tions within our computational accuracy. The results visualised in this manner do not suffer of projection effects. With this method it is also easy to extend our study to include the influence of different initial conditions such as different velocities or masses. These extensions will help us understand the chaotic nature of the three body systems both in much greater detail and in a more comprehensive way. We also discuss shortly the numerical sensitivity of general three-body problem and show that this may indicate the presence of the Arrow of Time within these systems.

2 DECAY TIME-SCALE AND FRACTALITY

We have considered the simplest initial state in an equal mass three-body system under Newtonian gravitation. The calculations start at rest and have no angular momentum. We have used in our calculations a fully chain-regularized Bulirsch-Stoer integrator (Mikkola & Aarseth 1990, 1993, 1996).

To visualize our simulations we use an extended version of an homology map (Agekian & Anosova 1967). In this coordinate system one body resides initially at $(0, 0)$, the second one is at $(1, 0)$ and the third one is at (x, y) . A shield shaped area contains all possible values of (x, y) , spanning in abscissa from 0.0 to 1.0 and in ordinate from

* E-mail:hlehto@utu.fi

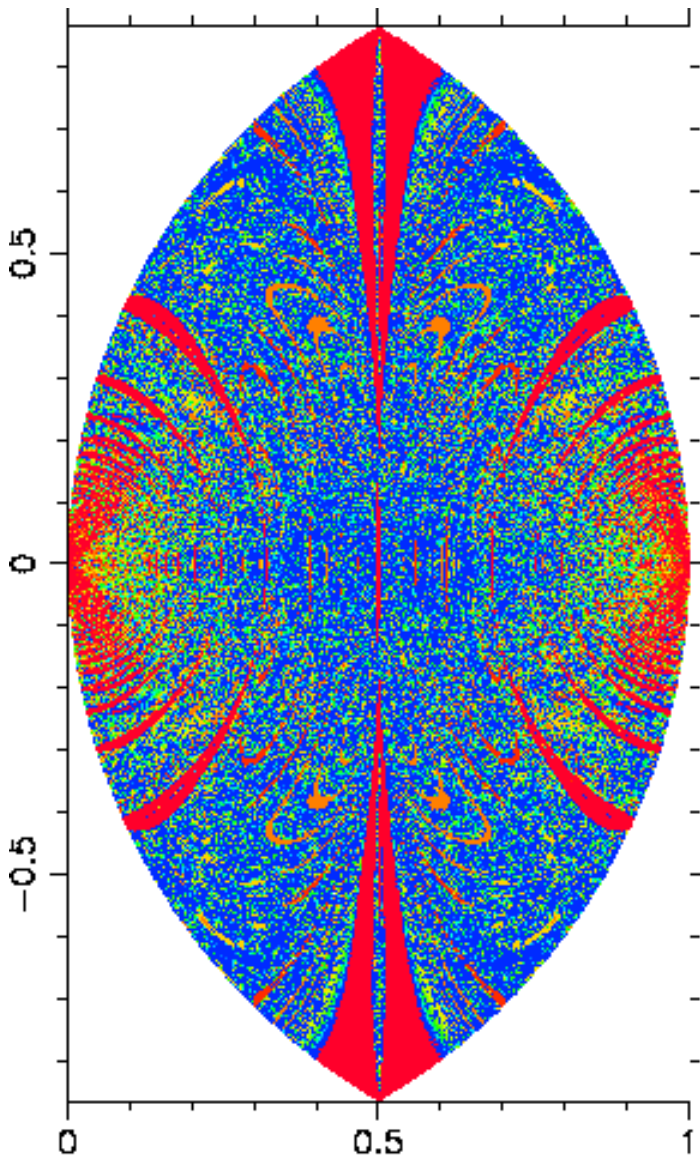


Figure 1. The life time of gravitational three body systems containing all possible of orbits that were initially at rest. The initial configuration of the three body system is such that one star is located at $(0, 0)$, the second one at $(1, 0)$, and the third one at a coordinate (x, y) . The colour pixel at (x, y) shows then the time elapsed from the initial configuration to the disintegration of the system under Newtonian gravitation. Red denotes short lived systems, decaying within one crossing time, orange systems decaying before two crossing times, etc. The dark blue colours represent systems with the longest lifespans (over 13 initial crossing times). The pixel size is $1.25 \cdot 10^{-3}$. The image of the complete shield is symmetric, because we start with all three objects at rest. Note the wide resonant bands causing a rapid disintegration of the system. Also note how narrower bands abound between wide bands.

$-\sqrt{3}/2$ to $\sqrt{3}/2 \approx 0.866$. A three body configuration can thus be unambiguously specified by a single point in this map. The unit time-scale of our ($G = 1$) system is $t = \frac{1}{2\pi}(R/1\text{AU})^{3/2}(M/M_{\odot})^{-1/2}$ years, where R is the longest separation of the initial triangle and M is the mass of the objects.

Except for a few double or triple collision points (Umehara & Tanikawa 2000), all our three-body systems will eventually break up. The escaping body will have a non-negative total orbital energy. To define the breakup time of the system we also require that the escaping body must be at a distance of $r \geq 1$ from both remaining bodies. This is necessary because during strong interactions the total en-

ergy of a body may, as expected, become momentarily highly positive.

Because the escaping body often has only a mildly positive energy and because the quantity we measure is time (the conjugate coordinate of energy in phase space), our measurement is in some respect analogous to a phase space cross-section of a triple system.

The lifetime of the system may now be plotted as a function of the initial configuration. A complicated structure emerges (Fig. 1). As a curiosity, the overall pattern shows a nice resemblance with a traditional African Maasai warrior shield (see e.g. Huntingford 1961). Since we consider an equal mass system, there is a left-right symmetry in the

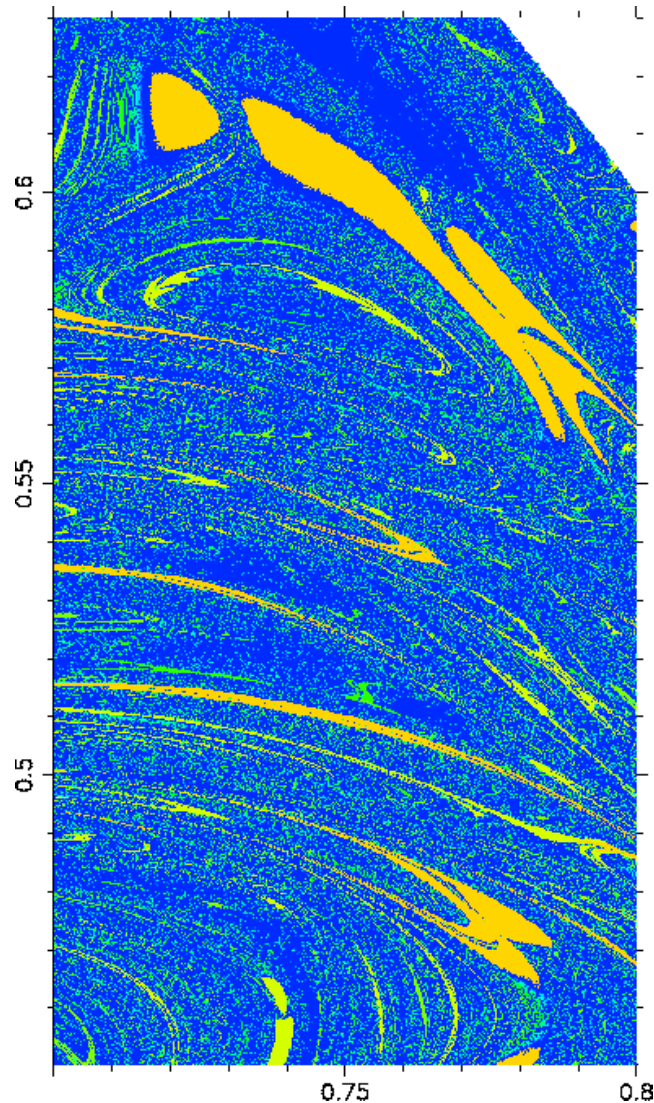


Figure 2. The life time of gravitational three body systems, a zoomed in image of Fig. 1. The pixel size here is $2.5 \cdot 10^{-4}$. Colours as in Fig. 1. Note how this region appears quite 'stable' in Fig. 1, yet in this image it has broken into hundreds of narrow bands of instability. Note that the large yellow area breaks into three major parts. This is a universal feature for the loops. They correspond to the different object being ejected from the system. The point where these three parts meet is a triple collision point. The boundary of the yellow area is sharp from inside. If one approaches the boundary from the outside one encounters a number of orbits growing in density and stability as one approaches the sharp boundary.

diagram. The non-zero initial velocity, eg. for the third body will in general break the up-down symmetry.

2.1 Resonances

On the largest scales the following regions of instability can be identified. A configuration initially close to an isosceles triangle (1:1 resonance) is generally highly unstable (the vertical red band close to the vertical symmetry line of the map). Systems close to odd-digit orbital resonances (1:3, 1:5, 1:7 etc) are highly unstable, because a very close approach takes place at the first close triple encounter. These are the bands growing denser towards the left and the right corners of the map. Note also the branching of the 1:7 and higher order resonances. Furthermore, resonances 1:2, 1:4 etc. are completely missing, because the phase in these cases is not

favorable at the first close encounter to a rapid break-up of the system (Saslaw & Valtonen 1974). Systems breaking up due to the second close interaction show up as long orange arcs. The family of these arcs starts from the central part of the map and extends towards the edges of the map. A second system of arcs between the previous set and the 1:3 resonance is also due to the odd resonances at the second encounter. A band due to similar resonances (nearly vertical bands) can be seen at the edge of the 1:1 resonance.

All the major resonances appear to avoid a sea of apparent tranquility around the surroundings of $(x, y) = (0.7, 0.5)$ and the corresponding points in the other quarters of the shield.

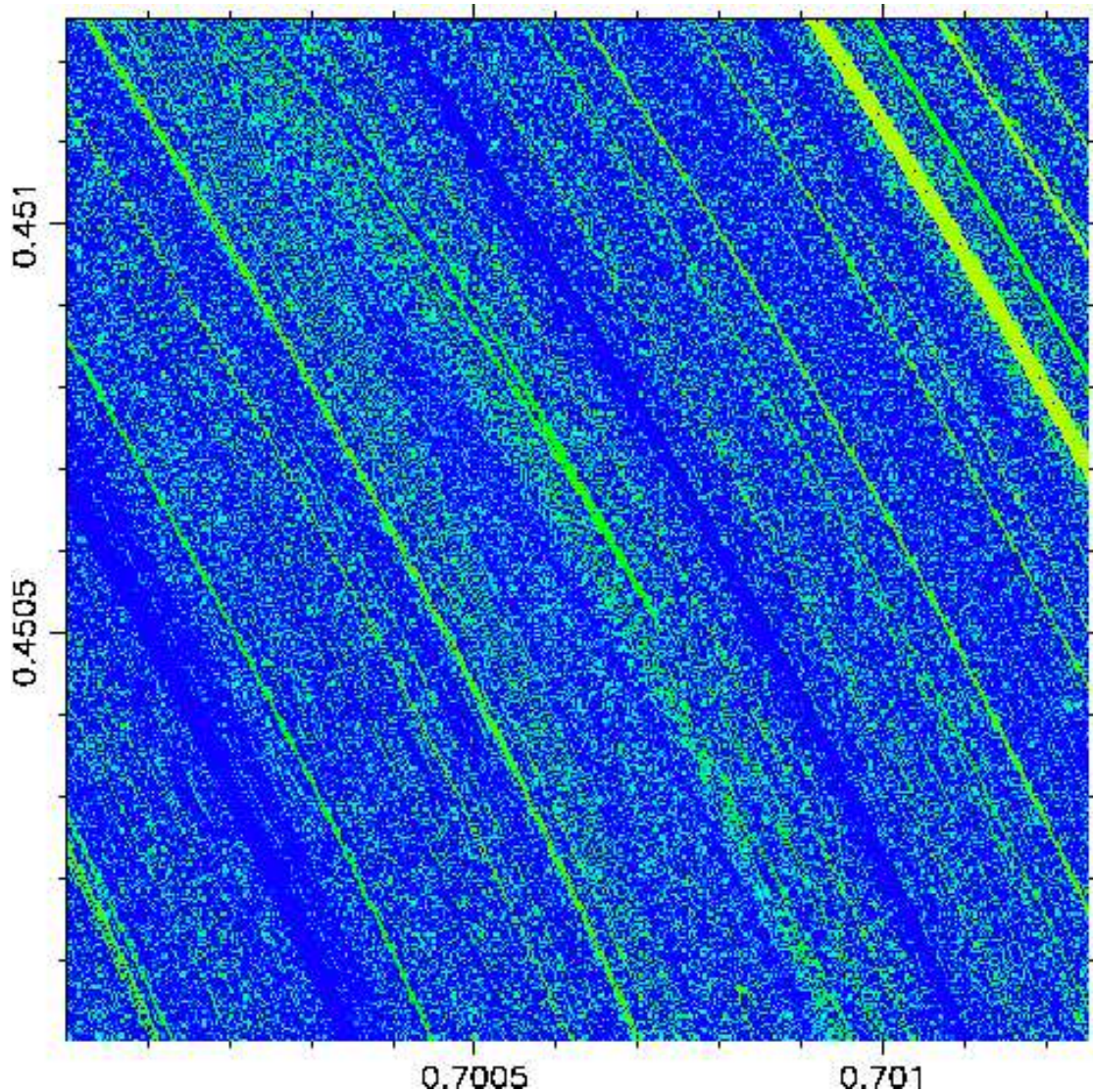


Figure 3. The life time of gravitational three body systems, a zoomed image of Fig. 2 showing the smaller details. The pixel size here is $3.125 \cdot 10^{-6}$. The colour scale is linear and is extended to 20 crossing times. The dark blue colours show orbits that have not disintegrated in 20 crossing times. The light green band in the right upper corner of this image corresponds to a disintegration in about 7 crossing times.

2.2 Local structure

Locally the boundaries of these resonance regions are sharp from the inside. Approaching the boundary from outside one encounters ever denser loops and stripes. This structure appears selfsimilar and locally fractal.

Areas of higher stability are also present in Fig 1. These fall into two categories. The first set are isolated deep trenches on large scales at about $(0.70, 0.64)$ and $(0.65, 0.15)$ and at respective symmetric points of the shield. The second set better visible on small scales are configurations just outside some instability regions e.g. around the upper branch of the 1:7 resonance at $(0.90, 0.23)$ or below the yellow eye at $(0.75, 0.60)$ and the corresponding symmetric points.

Figures 2 and 3 show progressive levels of zooming into these areas. Figure 3 represents a 5 by 5 pixel area in the lower left corner of Figure 2. The width of the stripes seen in Figure 3 is comparable to the resolution element or

$3.125 \cdot 10^{-6}$. These stripes are more easily seen if the image is viewed at a small angle. It is clear that a tiny change in the initial conditions may cause a substantial difference in the lifetime and in the evolution of the system. Further details of the orbital behavior within these areas is beyond the scope of this paper, except that we may state that these configurations appear to be more stable.

2.3 Global fractality

To investigate the ratio of stable (locally homogeneous) regions to the chaotic regions we compared, t_o , the ejection time of an orbit to t_{med} , the median of 8 nearby orbits located on a rectangular grid with total width of $3.75 \cdot 10^{-3}$. The eight configurations are separated by $\epsilon = \pm 1.25 \cdot 10^{-3}$ in each of the x and y coordinates from the initial point.

If $|t_{med} - t_o| \leq 0.5$, we considered the point to have an locally homogeneous neighbourhood. Otherwise it was

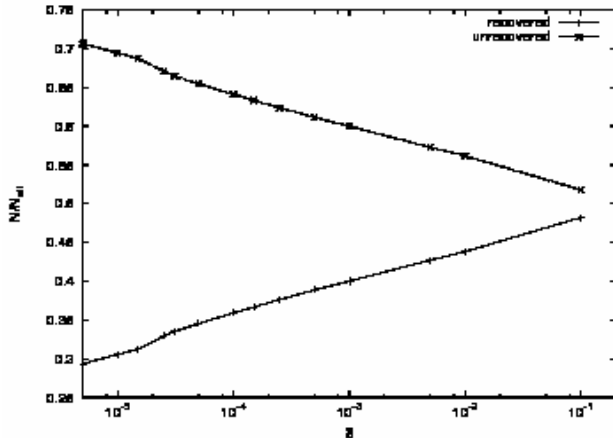


Figure 4. The number fraction of recovered and unrecovered orbits as a function of required accuracy δ . At around $\delta = 10^{-5}$ one come to the limit of decimals in the result files.

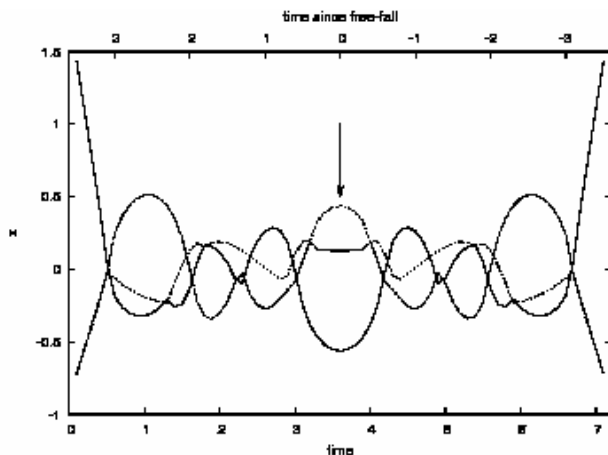


Figure 5. An example of a time symmetric orbit. The orbit is calculated first from free-fall position to escape (part not shown here) and then correctly back in time to the original free-fall situation which is found at $t = 3.6$ and indicated by an arrow. Finally the integration was continued until the system breaks up again at $t = 7.2$.

considered to have high sensitivity to initial conditions, a characteristic of chaos. Of the 21 699 cases compared in this manner 6212, or $p_\epsilon = 28.6$ per cent were in locally homogeneous. The remaining 71.4 per cent of positions turned out to be highly sensitive to initial conditions at this resolution implying that on the scale of $\epsilon = 1.25 \cdot 10^{-3}$ the fractal area covers about 71.4 per cent of all the systems. The implication of this is that if one is able to determine the initial state of a triple system to an accuracy of ϵ , one will, with the stated probability, be unable to tell the time-scale of the ejection of the third body to within half a crossing time.

If our image is fractal one should find more and more (local) order as one decreases the resolution element. This will be difficult to do due to restrictions in computation time. We can increase the resolution and see if the amount of local homogeneity decreases in a self similar way. For bin sizes 1, 2, 3, 4, 5 and 10 times the original one we find a decrease in local homogeneity, p_ϵ , 28.6, 16.8, 14.9, 13.8, 13.5 and 8.6 per cent, respectively. To within measurement

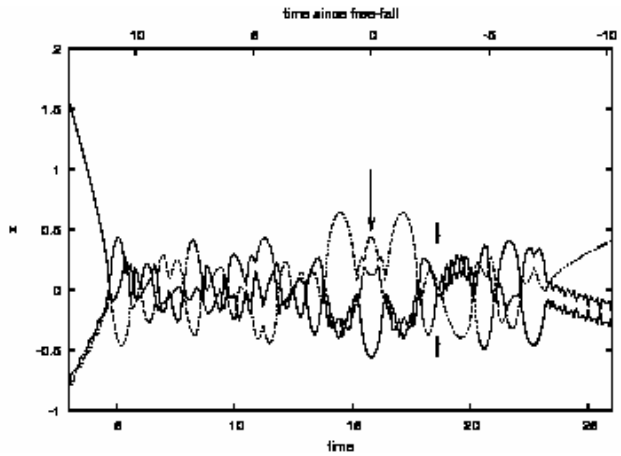


Figure 6. An example of an orbit which is asymmetric with respect to time. This orbit is also traced back to its free-fall moment at $t = 15.8$ (marked with long arrow) but the motion after this differs from the previous history at $t = 18.6$ (marked with two arrows) leading in this case dramatically different break up.

errors $p_\epsilon \propto \epsilon^{-0.5}$. We find the same exponent if we study the detailed areas shown in Figures 2 and 3. The Hausdorff dimension (Hausdorff 1919) of our image is thus

$$D_H = 1.5.$$

3 TIME REVERSAL AND THE ARROW OF TIME

The initial conditions we choose for our systems have the important mathematical property that the orbits we calculate are time symmetric with respect to the origin. This implies that the triple systems we calculate are transient in the sense that the body expelled must have been once captured by the very same bodies forming the final binary system (and even in the very same phase but with an opposite sign!). Physically this is not quite true, because even a small disturbance to the system would cause the system to loose this property. This also implies that a simple time reversal at the time of escape will not be a useful indicator of the errors involved in these calculations.

It is possible that the initial conditions are not recovered by two reasons: the calculations may not be accurate enough, and errors accumulate to the extent where the initial conditions are missed on the way back. The second possibility is that the calculation is accurate enough, but the individual system is so sensitive that it is practically impossible to find the initial conditions again. See Aarseth et al. (1994) for a discussion of predictable and non-predictable orbits.

To ensure independence from the method our calculations were done with two different methods. The method uses a code consisting of a Bulirsch-Stoer integrator with the chain regularization algorithm (Mikkola & Aarseth 1993). The second code uses a simple leapfrog integrator to logarithmic Hamiltonian (Mikkola & Tanikawa 1999). Results obtained are in agreement but in analysis we prefer the latter code because of its constant stepsize.

The orbits were calculated in few stages. First a for-

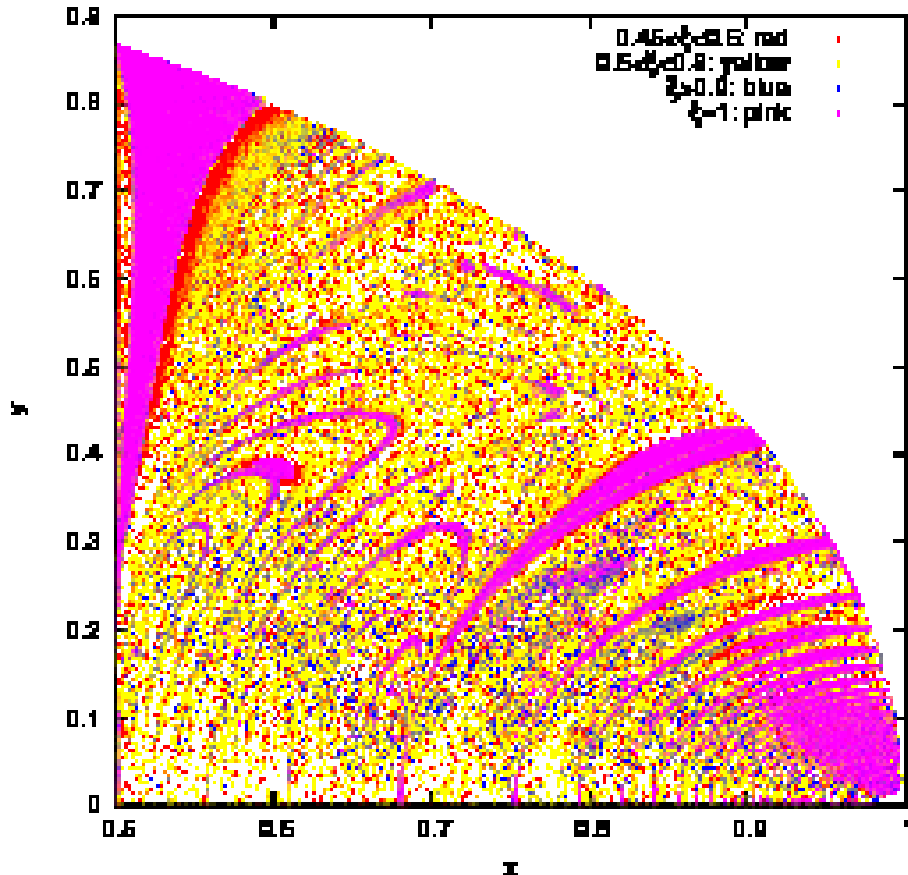


Figure 7. The homology map for most recovered orbits. The structure of the map is very similar to the one obtained by ejection times in Fig. 1. Here the colour indicates ξ , the amount of time symmetry, for each orbit. Notice how this value tends to increase when initial configuration depart from the resonance bands.

ward integration was carried out until one of the bodies escapes. Here one should notice that criterion for recognizing an escape is not trivial. An escape is suspected if the ratio between the semi-major axis of one body orbit and the semi-major axis of the binary (i.e. two bodies close to each other) is large enough. We have selected this ratio to be 100. In addition to this requirement the system has to fulfil one of the two following conditions. An escape is identified if the third body is on an hyperbolic orbit *and* is moving away from the binary. Alternatively, if one of the bodies gets so far that the ratio exceeds ≥ 2000 we consider this an escape, even though a proper hyperbolic orbit is not present. These escape criteria follow Anosova (1986), which includes also a list of different possible escape criteria. We have also tried smaller values for the escape criteria with no apparent effect on our results.

At the second stage the escape velocities were reversed and a reverse orbit was calculated until the system reached its initial conditions again. After that the simulation has carried on until the system breaks up again.

The definition of when the initial conditions has been recovered depends on the accuracy of the computer and software. We find that by using double precision we can expect results to be correct at least with accuracy $\sim 10^{-7}$. To avoid rounding errors we consider only five significant digits. Therefore we require that the separation between original

initial state and its recovered counterpart must be less than $\delta = \pm 5.0 \cdot 10^{-5}$. The choice of this limit affects naturally the ratio of the recovered and unrecovered orbits. The ratio is shown in Figure 4 where different values of δ has been applied to the dataset.

If one would have an infinite accuracy one would obtain an orbit where the motion is exactly the same before and after the free-fall moment – in the other words the orbit is time symmetric. This is a fact which is based on the equations of motion. However, in most cases in our numerical calculations this is not the case even though the free-fall moment can be recovered: most orbits actually forget their past after the free-fall moment producing an asymmetrical time evolution. This difference is illustrated with examples in Figure 5 for time symmetric and Fig. 6 for time asymmetric orbits. We define a new quantity ξ as time ratio of the a recovered part to the orbit's time of disruption t_{tot} . If $\xi = 1$ the orbit is exactly the same in the past and in future from the free-fall moment. In Fig. 7 the value of ξ is presented for each orbit identified by its initial position on the homology map. The orbits marked by pink colour represent the totally symmetrical evolution while other colours indicate binned values of ξ for asymmetric orbits. In red pixels the length of the symmetric part is between 0.45 – 0.60 of t_{tot} . In the yellow pixels symmetry covers 0.6 – 0.9 of t_{tot} and at the blue pixels the orbit is over 90 but less than 100 per

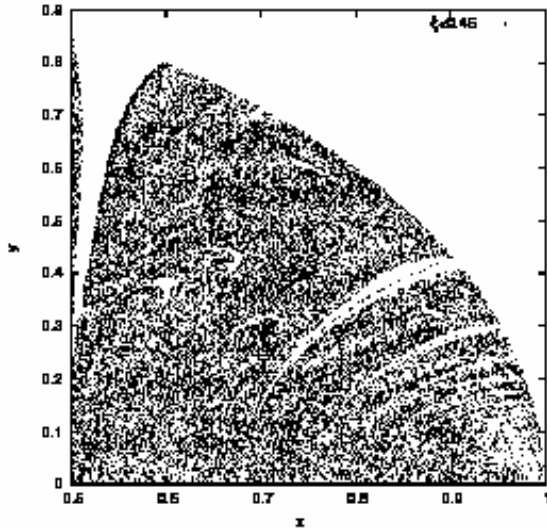


Figure 8. The homology map for recovered orbits with $\xi \leq 0.45$. These orbits do not form any grouping as seen for higher values of ξ in Fig. 7.

cent symmetric. The white areas – distributed quite equally everywhere on the map outside the resonances – loose their symmetry faster than within 0.45 of t_{tot} or they represent cases where the orbit has not been recovered. The bins for ξ in Fig. 7 are based on the distribution of orbits in Figure 9 which we will discuss later.

According to Fig. 7 one will find the exactly time symmetric behaviour within resonance areas where orbits have relatively short lifetimes. But is there any relation between the lifetime of the asymmetric orbits and their sensitivity to the numerical errors? This question is answered in Figure 9 where we present the amount of symmetry, ξ , as a function of disruption time of the system. It appears that the population of asymmetric orbits are divided into two, partially overlapping, groups. Both of these groups have distinctive functional form $\xi_i(t_{\text{tot}}) = a_i t_{\text{tot}}^{-n_i} + b_i$ and these sets appear to have quite sharp edges on the minimum side. Population I ($\xi \gtrsim 0.45$) seems to be direct continuum of time symmetric orbits ($\xi = 1$) while the lower edge of the curve has approximately parameters $a_1 = 0.5, n_1 = 0.7$ and $b_1 = 0.47$. These orbits appear to be located just outside the resonance areas on the homology map and the value of ξ increases when the initial configuration moves farther from the resonance bands.

Most orbits however belong to population II ($0 < \xi < 1$) which is quite equally distributed over the homology map, clearly further from the resonance bands. The lower limit of ξ in this population obeys approximate relation $a_2 = 2.5, n_2 = 0.9$ and $b_2 = 0$. On the homology map (Fig.8) this population is strongly intermixed with non-recovered orbits but the latter ones do not show any clear functional form for $\xi = \xi(t_{\text{tot}})$.

We have found out that even in quite a simple dynamical system such the classical equal-mass free-fall three-body problem, actually the Arrow of Time shows up. Considering the analytical point of view the autonomous form (i.e. no explicit time dependency) of the equations of motion and the lack of dissipation suggest that this arrow would not

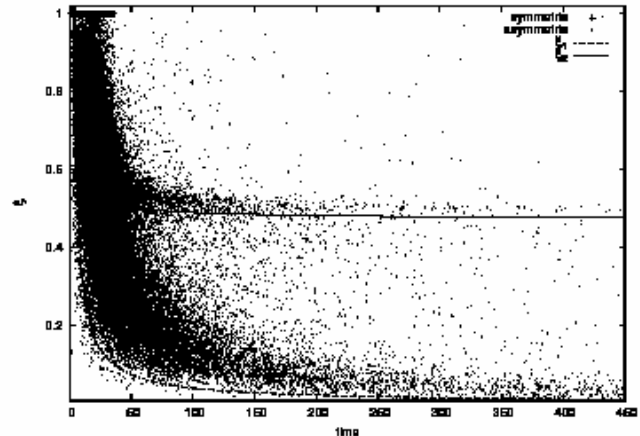


Figure 9. The symmetry, ξ , of the orbit as a function of the lifetime. The functional forms $\xi_1(t_{\text{tot}})$ and $\xi_2(t_{\text{tot}})$ for two distinctive populations of time asymmetric orbits are also shown (see text). Totally time symmetric orbits form short horizontal line at $\xi = 1$.

be there if we could solve the problem exactly. However, in nature totally unperturbed systems do not exist and even a minute perturbation, just like a small computing error, is adequate to define a definite sense of time.

How do we find out what is the forward sense of time in the three-body problem? The answer is provided by the concept of entropy again. Not the classical Boltzmann entropy, but Kolmogorov-Sinai entropy (Kolmogorov 1958; Sinai 1959). This concept of entropy applies to small systems. It is related to the change of the volume of phase space occupied by systems which are initially very close to each other. It measures the loss of information about the initial conditions or the growth of disorder as time goes on. We have previously shown that Kolmogorov-Sinai entropy increases with time in the three-body problem, and that it thus tells us what is future, and what is past (Heinämäki et al. 1999). The Kolmogorov-Sinai entropy increases towards future time.

There are other examples of determining the sense of time in the three-body problem. In three-body scattering a single body collides with a binary, and after some orbital evolution, one of the bodies escapes and leaves again a binary. Let us say that the initial binary has zero eccentricity. The final binary has an eccentricity e that follows the distribution $f(e) = 2e$ (Jeans 1919; Heggie 1975). Thus the probability that the final binary escapes with zero eccentricity is zero. In a diagram depicting such a scattering event (see e.g. Hut & Bahcall 1983) it is immediately clear which is the direction of orbital motion even if it is not indicated. Although some of our orbits perform time symmetric past and future they resemble a minority in our ensemble and it is somewhat reasonable to consider the Arrow of Time in the universe as a statistical quantity. One may also ask if these time symmetric orbits really appear at all in true nature where small perturbations are always present.

The microscopic world consists of many small subsystems similar to the classical three-body system. It is our conjecture that our conclusions would apply also to such systems, and that Kolmogorov-Sinai entropy would actually provide the Arrow of Time for the microworld.

There have previously been a number of papers considering a relation between the Kolmogorov-Sinai entropy and the Boltzmann thermodynamic entropy. These studies, which have been done in other fields of physics. They have either tried to address the relation between these two quantities, albeit such relation still remains unknown, (see e.g. Latora et al. 1999; Baranger et al. 2001) or attempted to find a direct equivalence between the dynamical instability and the thermodynamic irreversibility (Elskens & Prigogine 1986; Yukalov 2003; Ruiz & Tsallis 2007). If these relations indeed exist, they endorse our conclusion.

4 NOISE ESTIMATES

Since noise estimates are difficult to perform in these kinds of systems. We followed the simpler practice of reducing the integration step by a factor of 2. We noticed only a slight sharpening in the boundaries, but no qualitative differences nor any unexpected quantitative differences.

A second strong test we have performed is for the robustness of the method. We ran a naïve simulation with non-regularized equations of motion but with a short variable steps of integration. The code is very different in nature from our main code. Yet the results are very similar showing the main resonant structures. On small scales similar fractal-like patterns appear as with our main code.

5 DISCUSSION

The results from Heinämäki et al. (1999) and Anosova (1986), suggested that a homology triangle-like representation is an ideal means to describe the evolution or the final solutions of a triple system, and that it would show structure both due to global and local sensitivity to initial conditions. The geometry of escape times which we have calculated shows rich structure featuring resonance bands at various levels and areas of apparent higher stability as well as areas with clearly a fractal structure.

The time-scales in question for solar mass objects and an initial length scale of $R = 1$ pc correspond to $t \sim 1.6 \cdot 10^7$ years. The implication is that triple stellar systems forming initially from distant stars may still be in a multiple system after a few tens of million years (the blue areas in Figure 1 imply time-scales $> 1.6 \cdot 10^8$ years). On the other hand one would expect stars being ejected by this method from young systems to form loose associations at the latest in about a ten million years. If the stars were closer ($R = 0.1$ pc) then the breakup times would be a factor 30 shorter. On the other hand if the stars were not initially at rest then these time-scales are likely to be somewhat longer based on previous work (see e.g. Saslaw & Valtonen (1974); Valtonen & Karttunen (2006)).

Galaxies at distances of ~ 1 Mpc, and with masses $M \sim 50 \cdot 10^9 M_{\odot}$ have a typical time-scale of $10^{10.5}$ years, so these are expected to be still these initial orbits, even if they were near the resonance configuration.

ACKNOWLEDGMENTS

This work has been funded by Finnish Cultural Foundation and Jenny and Antti Wihuri Foundation.

REFERENCES

- Aarseth S.J., Anosova J.P., Orlov V.V., Szebehely V.G., 1994, *Celest. Mech.*, 58, 1
 Anosova J.P., 1986, *Ap&SS*, 124, 217
 Agekian T.A., Anosova J.P., 1967, *SvA*, 44, 1261
 Baranger M., Latora V., Rapisarda A., 2001, *Chaos Solitons and Fractals*, 13, 471
 Elskens Y., Prigogine I., 1986, *PNAS*, 83, 5756
 Hausdorff F., 1919, *Mathematische Annalen* 79(1–2), 157
 Heinämäki P., Lehto H., Valtonen M., Chernin A.D., 1999, *MNRAS*, 310, 811
 Heggie D.C., 1975, *MNRAS*, 173, 729
 Huntingford G.W.B., 1961, *The Journal of the Royal Anthropological Institute of Great Britain and Ireland*, Vol. 91, No. 2., 251
 Hut P., Bahcall J., 1983, *ApJ*, 268, 319
 Jeans J., 1919, *MNRAS*, 79, 408
 Kolmogorov A.N., 1958, *Dokl. Acad. Nauk. SSSR*, 119, 861
 Latora V., Baranger M., 1999, *Phys. Rev. Lett.* 82, 520
 Mikkola S., 1994, *MNRAS*, 269, 127
 Mikkola S., Aarseth S.J., 1990, *Celest. Mech.*, 47, 375
 Mikkola S., Aarseth S.J., 1993, *Celest. Mech.*, 57, 439
 Mikkola S., Aarseth S.J., 1996, *Celest. Mech.*, 64, 197
 Mikkola, S., Tanikawa K., 1999, *MNRAS*, 310, 745
 Poincaré H., 1892, *Les Méthodes Nouvelles de la Mécanique Celeste*. Gauthier-Villars, Paris
 Prigogine I., Stengers I., 1984, *Order out of Chaos*. Bantam books, New York
 Ruiz G., Tsallis C., 2007, *Physica A*, 386, 720
 Saslaw W.C., Valtonen M.J., Aarseth S.J. 1974, *ApJ*, 190, 253
 Sinai Ya.G., 1959, *Dokl. Acad. Nauk. SSSR*, 125, 1200
 Umehara H., Tanikawa K., 2000, *Celest. Mech.*, 76, 187
 Valtonen M.J., Karttunen H., 2006, *The Three-Body Problem*. Cambridge Univ. Press, Cambridge
 Yukalov V.I., 2003, *Physica A*, 320, 149

This figure "Lehto1.png" is available in "png" format from:

<http://arxiv.org/ps/0805.2844v1>

This figure "Lehto2.png" is available in "png" format from:

<http://arxiv.org/ps/0805.2844v1>

This figure "Lehto3.png" is available in "png" format from:

<http://arxiv.org/ps/0805.2844v1>

This figure "Lehto4.png" is available in "png" format from:

<http://arxiv.org/ps/0805.2844v1>

This figure "Lehto5.png" is available in "png" format from:

<http://arxiv.org/ps/0805.2844v1>

This figure "Lehto6.png" is available in "png" format from:

<http://arxiv.org/ps/0805.2844v1>

This figure "Lehto7.png" is available in "png" format from:

<http://arxiv.org/ps/0805.2844v1>

This figure "Lehto8.png" is available in "png" format from:

<http://arxiv.org/ps/0805.2844v1>

This figure "Lehto9.png" is available in "png" format from:

<http://arxiv.org/ps/0805.2844v1>